Advanced Data Analysis for Geological and Engineering Hazard Study

Ray Ruichong Zhang

Abstract — This paper presents the rationale of an advanced data analysis, i.e., Hilbert-Huang Transform (HHT), for analyzing ground acceleration recordings and subsequently for studies of seismology and earthquake engineering. In particular, this paper first uses hypothetical and real wave recordings to illustrate features of HHT analysis in nonlinear, non-stationary data processing. It then examines causes of dominant HHT-based components of earthquake recordings as they relate to geological source, and engineering implications of HHT-based features of ground motion from the perspective of the motion's damage potential to civil structures.

Keywords — Hilbert-Huang Transform, Fourier Transform, Seismic Ground Recordings.

I. INTRODUCTION

Earthquake ground acceleration recordings are important for the following reasons:

(1) As the output in modeling earthquake wave motion and explaining earthquake phenomena in the earth, they can help understand such seismological issues as source mechanism, directivity influence, and soil dynamic non-linearity [1-6].

(2) As the input to geotechnical and structural engineering systems, they can be used to compute dynamic nonlinear responses and thus to evaluate seismic performance of those systems. This analysis can quantify earthquake impact on various engineering systems and aid in the seismic-resistant design and retrofit [1-4, 7-8].

Conventional data processing techniques, however, yield distorted, indirect, or incomplete information about ground motion that is inherently non-stationary and also likely the result of a nonlinear dynamic process. This might mislead subsequent use of the ground motion data in addressing many seismological and engineering issues.

Because of its ability to faithfully characterize nonlinear, non-stationary data such as in earthquake recordings, the Hilbert-Huang Transform (HHT) method [9-10] can provide an alternative tool for earthquake data analysis and subsequently its applications in studies of seismology and earthquake engineering, among others [22-25].

The HHT method consists of Empirical Mode Decomposition (EMD) and Hilbert Spectral Analysis (HSA).

Any complicated data set can be decomposed via EMD into a finite and often a small number of intrinsic mode functions (IMF) that admit well-behaved Hilbert transform. The EMD explores temporal variation in the characteristic time scale of the data and thus is adaptive to non-stationary data processes. The HSA defines an instantaneous or time-dependent frequency of the data via Hilbert transformation of each IMF component. These two steps of data processing (i.e., EMD and HSA), namely HHT analysis, represent a generalized version of Fourier expansion. These two unique properties enable the HHT analysis to enhance the interpretive value of decomposed components (i.e., IMF or its grouped components) and their Hilbert spectra, relative to analysis of Fourier or wavelet components and spectra.

II. CHARACTERISTICS OF HHT DATA PROCESSING

In this section, we use hypothetical and real wave recordings to demonstrate the characteristics of HHT in analyzing nonlinear, non-stationary wave motion.
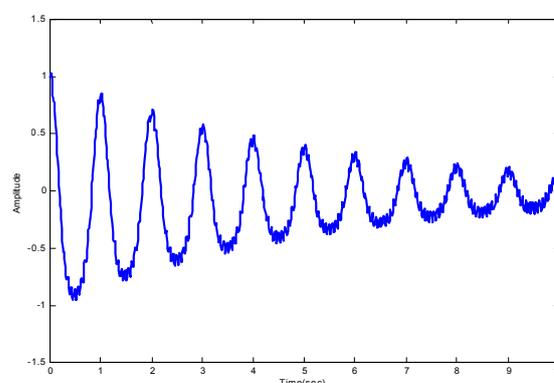
Fig. 1a A hypothetical wave recording.

Figure 1a shows a hypothetical wave recording $y(t) = y_1(t) + y_2(t)$ of decaying waves $y_1(t) = \cos[2\pi t + \varepsilon \sin(2\pi t)]e^{-0.2t}$ having intrawave frequency modulation around 1 *Hz* and high-frequency noise $y_2(t) = 0.05\sin(30\pi t)$. Note that the waves have a non-sinusoidal waveform with sharp crests and rounded-off troughs, which are representative of one type of water wave. Figure 1b shows the five IMF components decomposed from the data by EMD. The first and second components (c_1 and c_2) in Fig. 1b capture the noise and waves, while the other three (c_3 to c_5),

with negligible amplitude, represent the numerical error in the EMD process. By grouping the IMF components, EMD can also function as filters. Similar to high- and low-pass Fourier-based filters, the EMD-based high-frequency motion can be defined as the summation of first few IMF components, while the EMD-based low-frequency motion is the summation of the remaining IMF components. Figure 1c shows the EMD-based high- and low-frequency components which contain the 1st and the remaining four IMF components, respectively. The physical significance of the separation in Fig. 1c is a distinguishing here of the noise from true waves. Note that the choice of the number of IMF components for EMD-based motion is as subjective as the selection of cut-off frequency in Fourier-based filter. However, since IMF components typically have particularly useful interpretation such as in this example of wave recording and in many others [9]; the EMD-based motion likely contains information more appropriately characteristic of wave motion (e.g., waveform and peak characteristics). The Hilbert spectrum in Fig. 1d shows a clear picture of temporal-frequency energy distribution of the data, i.e., the true waves with intrawave frequency modulation around 1 Hz and a noise at 15 Hz.
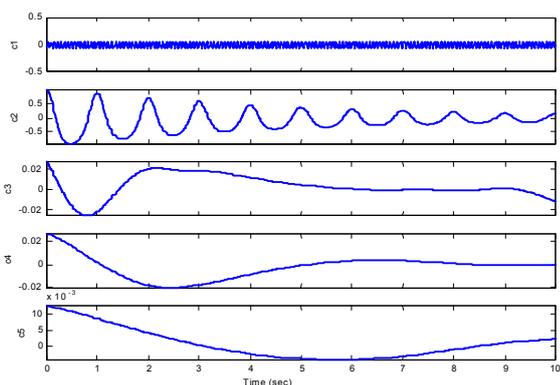
Fig. 1b   Five IMF components of the hypothetical wave recording in Fig. 1a.

As suggested in the above example, the Fourier- and wavelet-based components and spectra may not have as clear physical meaning as do the HHT-based ones. For detailed information, readers are referred to [11]. Conventional data processing methods, however, have the merit of a well-formulated basis in theory. Nevertheless, this study focuses on features of the HHT in analysis of nonlinear, non-stationary data for study of certain types of information that the conventional methods might not be able to reveal effectively, directly, or completely.
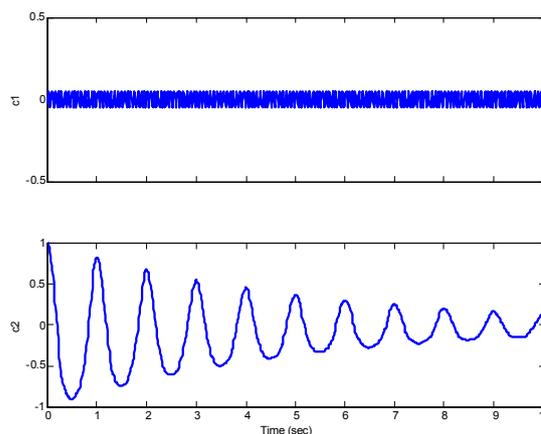
Fig 1c   EMD-based low-frequency (top) and high-frequency (bottom) components of the hypothetical wave recording.
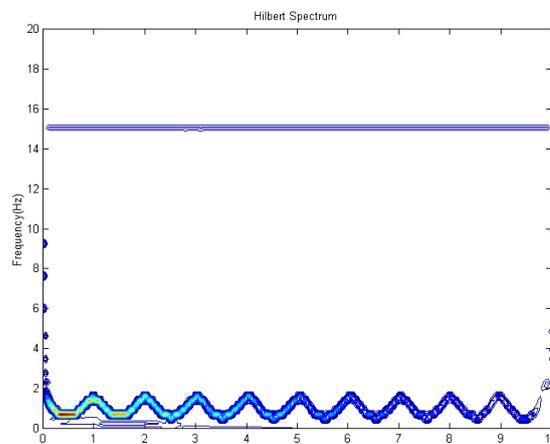
Fig 1d Hilbert spectra of the hypothetical wave recording.

An earthquake recording contains more complicated information than do the hypothetical waves in Fig. 1, as seen in Figs. 2a,b, which show respectively the north-south acceleration record of the 1999 Kocaeli, Turkey Earthquake at station YPT and its Fourier amplitude spectrum. Figure 2c shows the twelve IMF components decomposed from the original data by EMD, and Fig. 2d shows their corresponding Fourier amplitude spectra. Typically, earthquake data analyzed, such as those here, have around only ten IMF components, suggesting the efficiency of the EMD. As seen in Figs. 2c,d, each component emphasizes a different oscillation mode with different amplitude and frequency content. The first IMF has the highest-frequency content; frequency content decreases with increase in IMF component until the 12th IMF component, which is almost a linear function of time.
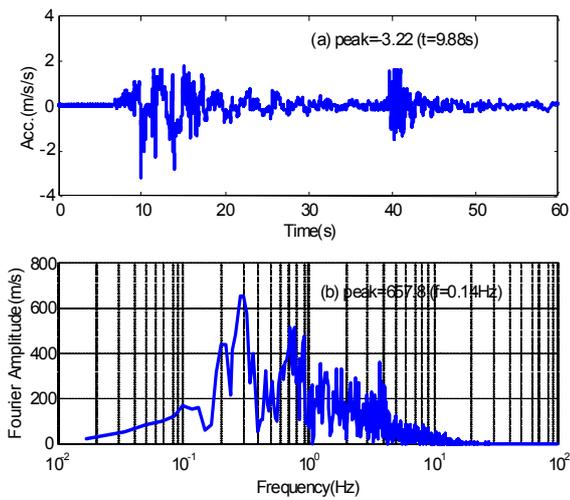
Fig. 2a,b (a, top) Recorded acceleration time history of north-south component at YPT in the 1999 Kocaeli Turkey earthquake, and (b, bottom) its Fourier spectrum.

Fig. 2c: 11 IMF components of acceleration time history at YPT.
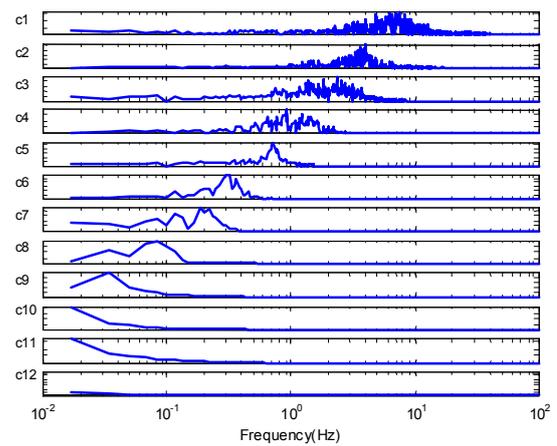
Fig. 2d Fourier Spectra of 11 IMF components of acceleration time history at YPT.
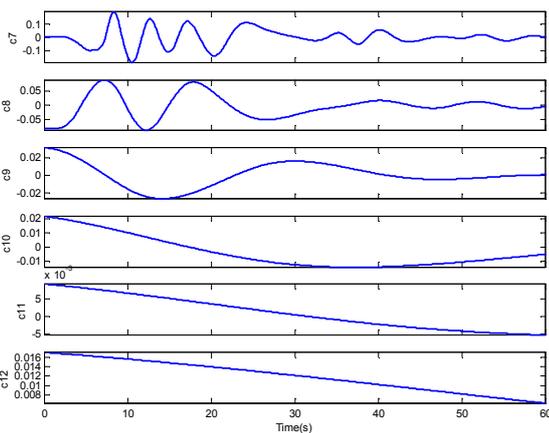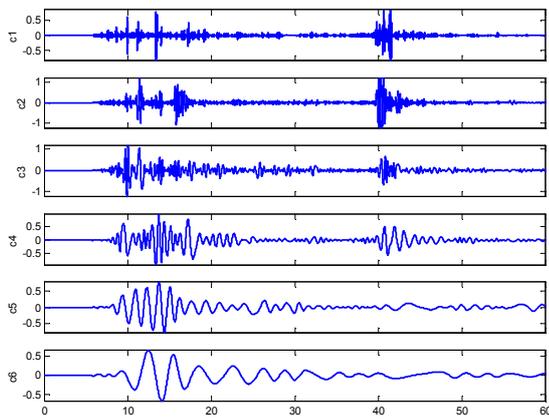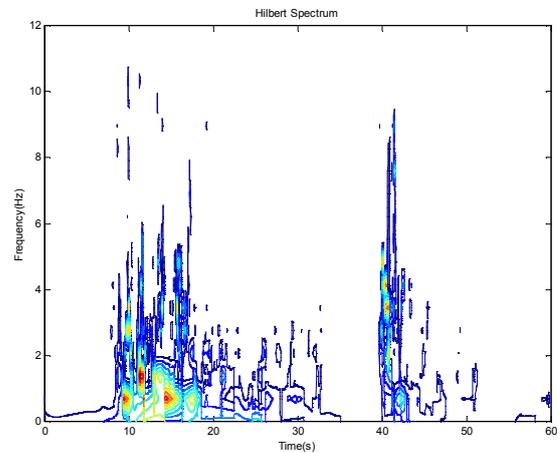
Fig. 2e   Contour plot of total Hilbert spectrum of recorded acceleration at YPT.
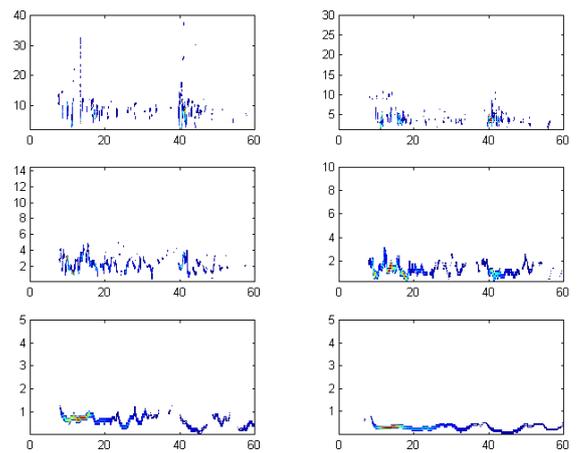
Fig. 2f Contour plot for the Hilbert spectra of the first (top left), second (top right), third (middle left), fourth (middle right), fifth (bottom left), and sixth (bottom right) IMF component of an acceleration recording at YPT.

Depicted in Fig. 2e is the total Hilbert spectrum of the Kocaeli earthquake recording at YPT. It consists of the 11 individual Hilbert spectra of each IMF component, the first six of which are depicted in Fig. 2f. These figures show quantitatively the temporal-frequency distribution of vibration characteristics in the ground motion recording. For example, Fig. 2e shows that the wave motion in time window 39-42 s contains more high-frequency energy than do other windows, consistent with visual observation of the original data in Fig. 2a. By examining Fig. 2f, one finds that the higher the IMF component, the less the variation in frequency content of the corresponding Hilbert spectra or energy distribution. The potential exists for the Hilbert spectra to provide a useful quantitative measure of a motion's input energy to structural systems.

III. CAUSES OF HHT-BASED MOTION COMPONENTS

Since all the IMF components extracted from acceleration records are the result of seismic waves generated by the seismic source and propagating in the earth, they should reflect the wave characteristics inherent to the rupture process and the earth medium properties. To this end, we next use 1994 Northridge earthquake recordings to examine causes of IMF components as they relate to source mechanisms. The primary reason for selecting the Northridge earthquake is that its source models have been established using Fourier-based data analysis. The source models obtained from HHT data analysis of the recordings can be compared with existing source solutions, facilitating the physical interpretation of IMF components.

3.1 Traditional Source Inversion Solution

We first summarize the inversion study of the Northridge earthquake source, which will be used as a reference for the interpretation of IMF components. The fault size used in [12] is shown in Fig. 3; the fault has a strike of 122° and a dip of 40° to the southwest. The fault plane measures 20 km in length and extends from a depth of 5 km to 21 km for a downdip width of 24.89 *km*. The fault is discretized into 14 x 14 =196 subfaults, each of which has four parameters: two slip weights (for rakes of 55° and 145°), rupture time, and rise-time.

A hybrid search algorithm is used to solve the nonlinear problem of calculating slip amplitude, rake, rise-time, and rupture time on a finite fault for the Northridge earthquake source. This requires information contained in earthquake records and pertinent synthetics. The earthquake records consist of a set of 35 two-horizontal-component ground acceleration records, one of which is shown in Fig. 4a. The distribution of recording stations is shown in Fig. 3. These 70 acceleration records are first corrected for the response of the instrument and then integrated to velocity, band-pass filtered from 0.1 to 1 Hz, and re-sampled at a time step of 0.1 s. The synthetics, i.e., the responses of seismic waves in a layered half-space to a point dislocation source, are calculated using the discrete-wavenumber/finite-element method [13], and then band-pass filtered from 0.1 to 1 *Hz*. Two different soil models

were used in synthetics, one for rock sites and the other with slower surface velocities for soil sites.
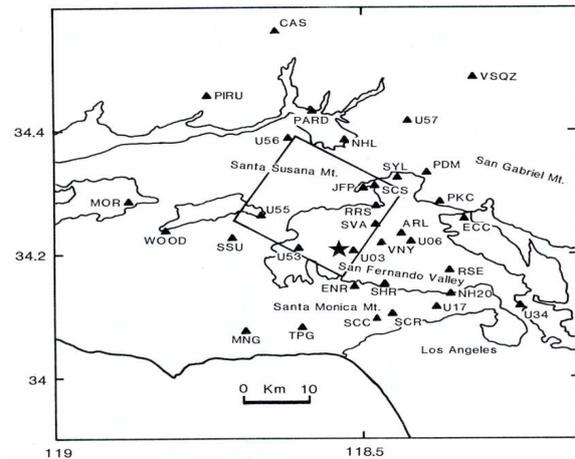
Fig. 3 Map of strong-motion stations (solid triangles) used in the inversion for slip, rupture time, and risetime. The surface projection of the model fault plane is indicated by the heavy box. The mainshock epicenter is given by the star [12].
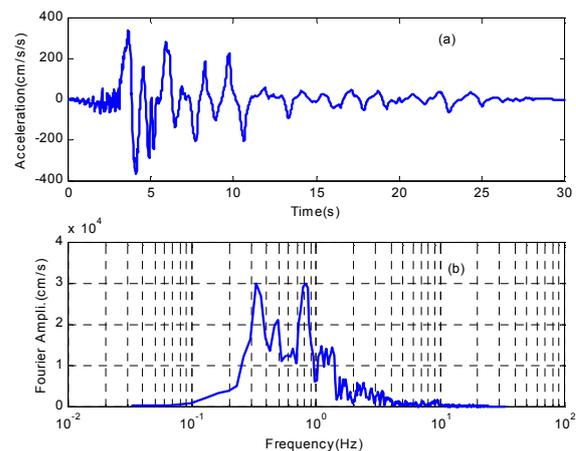
Fig. 4a,b (a, top) Recorded ground motion at station SCS1 in the 1994 Northridge earthquake, (b, bottom) its Fourier spectrum.
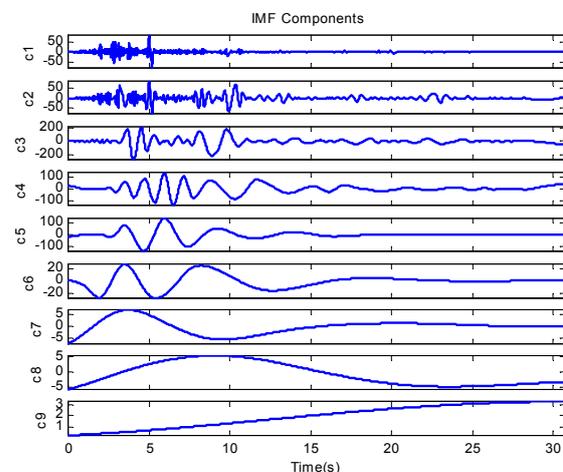
Fig. 4c Nine IMF components of acceleration recording at station SCS1.

Shown in Fig. 5 are the source inversions, i.e., the spatial distributions for the slip amplitude, rake, rupture fronts, and rise-time on the given finite fault. Basically, four regions of larger amplitude slip are identified in Fig. 5a: one for the hypocenter at a depth of 17 *km* (S1), a second west of the hypocenter at about the same depth (S3), a third updip from the hypocenter at a depth of 10 *km* (S2), and a fourth updip from the hypocenter and to the northwest (S4). Fig. 5d, together with Figs. 5a and 5c, shows that the slip near the hypocenter (i.e., S1) has a short rise time of 0.5 *s*, which increases to 1 s for the S3 and S2 and 1.5 s for the S4, as the major slip areas and rupture fronts are removed from the hypocentral region. This implies that slip region S1 will generate higher-frequency waves, S2 and S3 generate the moderate-frequency waves, and S4 generates lower-frequency waves.

to the seismic source (e.g., wave scattering in the heterogeneous media), and all the other IMF components (i.e., c6-c9) have small amplitudes compared with the four components used. The selected IMF components are then band-pass filtered with their own dominant frequency band, and re-sampled at a time step of 0.05 *s*. Finally, each set of these four IMF components is used as the observation data.
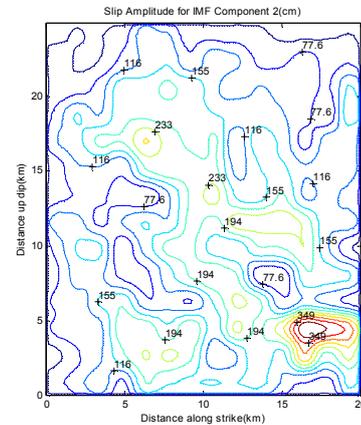
Fig. 6a Contour plot of slip amplitudes (*cm*) over the fault, corresponding to the second IMF components of recordings.
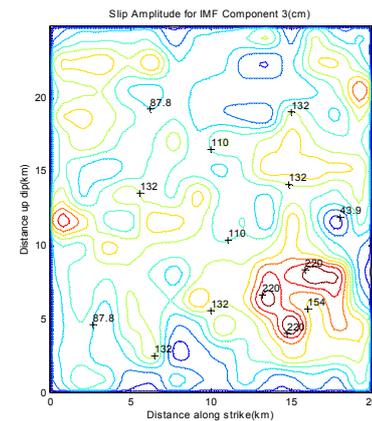
Fig. 6b: Contour plot of slip amplitudes (*cm*) over the fault, corresponding to the third IMF components of recordings.

Fig. 5 Plots of (a) slip amplitude (*cm*), (b) rake, (c) rupture fronts at 1-*s* intervals, and (d) risetime at 0.5-s contours for the preferred nonlinear, hybrid global search inversion [12].

3.2 HHT-based Source Inversion Solution

To provide physical interpretations of IMF components as they relate to the source mechanism, this study follows closely the techniques and pertinent fault information used in [12], but with different data analysis of recordings.

Specifically, instead of using velocity recordings for the inversion database, this study uses IMF components of the same 70 acceleration records as the database. These records are first corrected for the response of the instrument and then decomposed into IMF components. Typically, each record is decomposed into around eight or nine components (Fig. 4c). This study uses four IMF components (i.e., c2-c5) for investigation since the first highest-frequency IMF component likely contains information that is not simply or easily related

Fig. 6c Contour plot of slip amplitudes (*cm*) over the fault, corresponding to the fourth IMF components of recordings.
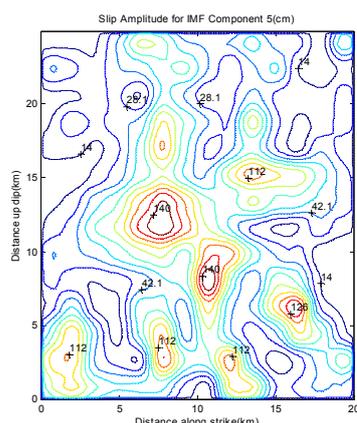
Fig. 6d Contour plot of slip amplitudes (*cm*) over the fault, corresponding to the fifth IMF components of recordings.

Figures 6a through 6d show the spatial distributions of slip amplitude over interpreted fault plane, each of which corresponds to the second through fifth IMF components of recordings. In comparison with Figs. 5a through 5d, we observe the following.

(1) The large slip amplitude regions shown in Figs. 6a through 6d are located at almost the same regions as those in [12] (i.e., S1, S2, S3 and S4 in Fig. 5a), suggesting that wave motion in each IMF component corresponds to a different aspect of the source.

(2) The large slip amplitude region in Fig. 6a, corresponding to the second IMF components, is essentially the first large slip amplitude region near the hypocenter in Hartzell's study (see S1 in Fig. 5a). As indicated above, S1 has the shortest rise-time (see Figs. 5a,d) and thus generates the highest frequency waves among the four regions (S1, S2, S3 and S4). The second IMF component also has the highest frequency content among the four IMF components we used. Therefore, the second IMF component is likely the wave motion generated by the main source near the hypocenter, with high-frequency content that might be related to a large stress drop with the initiation of the earthquake.

(3) The rupture with large-slip region in Figs. 6a through 6d progresses to the northwest from the hypocenter with the IMF components changing from the second (c2) to the fifth (c5). Since the frequency content in c2 to c5 is decreasing (see Fig. 4c), these four figures indicate that seismic waves are generated sequentially from dominant short-period signals to main long-period signals as the rupture propagates.

(4) Since each IMF component extracted from a recording may be associated with a different local characteristic time scale of the recording data, the seismic waves generated in the source (or specifically the rupture process) can be assessed from the observed time scale of waves. In particular, all kinds of waves with different time scales are generated as the seismic rupture propagates. They propagate and scatter through the earth media and constitute the complicated recorded ground motion at the stations with mixed time scale information. Since this mixed time scale information in recordings can be recovered by the EMD via IMF components, the whole rupture process can be reconstructed.

(5) This interpretation of the IMF components is based on only the time scale of waves generated by a source. Therefore, it is limited and biased. Actually, an earthquake recording results from both a rupture process in the source and wave propagation in the earth (linear or nonlinear), and thus is influenced by various scales of waves (e.g., spatial scales). Nevertheless, the above study suggests that the IMF components can contain information that sheds light on aspects of the earthquake process.

IV.   ENGINEERING IMPLICATIONS

A motion's potential to cause structural damage or specific responses can be measured with such recording features as peak ground acceleration (PGA), peak ground velocity (PGV), and velocity-based pulse-waves. They are, however, not as direct a measure as the EMD-based low-frequency acceleration (which we should call *EMD-low* measurement/acceleration) and its peak. The EMD-high measurement is defined as the summation of first few IMF components, while the EMD-low measurement is the summation of the remaining IMF components.

For illustration, we examine a pair of near-source Kocaeli earthquake recordings to see how the features of the EMD-low measurement are related to structural damage in general and the response spectra of linear, single-degree-of-freedom (SDOF) system in particular. The two recordings are the east-west acceleration at SKR (3.3 *km* from the surface rupture) and north-south acceleration at YPT (4.4 *km* from the fault). Note that the north-south acceleration at SKR is not available and the north-south acceleration at YPT has a larger PGA than does the east-west one.

Figures 7a and 8a show that the PGA at SKR, 407 cm/s^2, is much larger than the 322 cm/s^2 at YPT. Their velocity response spectra shown in Fig. 9, however, are just opposite to the PGA values for most civil structures (with fundamental period longer than 0.5 *s*, exemplified as medium- to high-rise or super-high buildings). This is because the PGA at SKR is associated with more high-frequency content than that at YPT, and the influence of the high-frequency motion component is typically less than that of the low-frequency motion component in structural dynamic responses.

4.1   Characteristics of EMD-low recordings

Since high-frequency motion components have generally less impact on most medium- to long-period civil structures than the low-frequency ones, we can remove them from the recordings in our study at this stage. Specifically, we examine the features of EMD-low measurement (excluding the first three high-frequency IMF components) for their relationship to structural responses. As shown in Figs. 8c and 7c, the peak of EMD-low measurement at YPT is 157.3 cm/s^2, larger than 134.1 at SKR. This is opposite to the measure of PGA of the original recordings, but consistent with the response spectra for

periods longer than 0.5 s in Fig. 9. Fig. 9 also shows that the EMD-low measurements generate response spectra close enough to those in the original recordings for structures with periods longer than 0.5 s, indicating that the EMD-low measurements capture well the influences of earthquake motion on most civil structures.
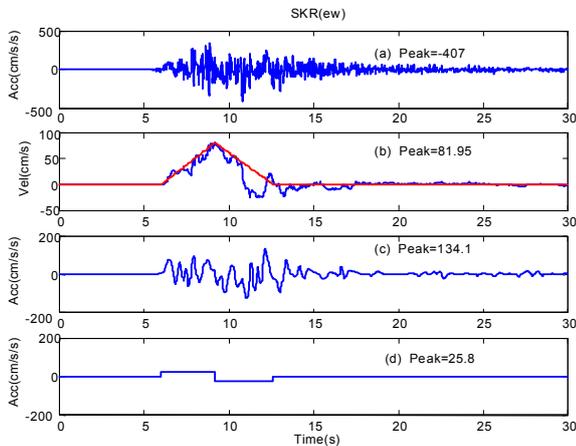
Fig. 7a-d (a) Acceleration recording in east-west component at SKR, 3.3 km from the fault, (b) Velocity time history in a curve line by integrating once the acceleration in (a) and a triangle-pulse approximation in a straight line, (c) EMD-based low-frequency acceleration (i.e., excluding the first three IMF components), and (d) acceleration obtained by differentiating once the triangle-pulse velocity in (b).
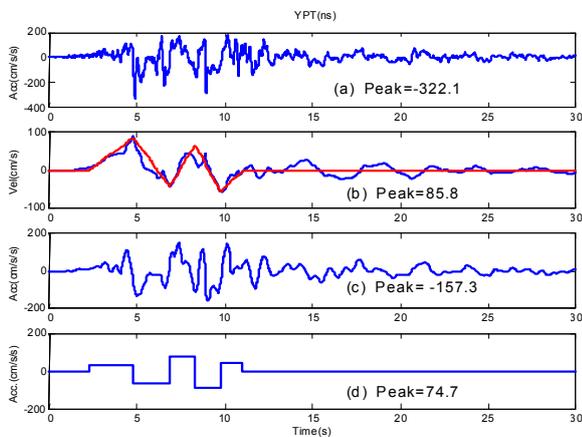
Fig. 8a-d (a) Acceleration recording north-south component at YPT, 4.4 km from the fault, (b) Velocity time history in a curve line by integrating once the acceleration in (a) and a triangle-pulse approximation in a straight line, (c) EMD-based low-frequency acceleration (i.e., excluding the first three IMF components), and (d) acceleration obtained by differentiating once the triangle-pulse velocity in (b).

To further clarify the close relationship between EMD-low measurement and structural response, we investigate the temporal-frequency seismic energy distribution of the two measurements through their HHT-based Hilbert spectra in Figs. 10a,b. In the frequency range 0 to 0.45 Hz in Figs. 10a,b, the EMD-low measurement at YPT contains primary energy

during the time periods 5-9, 12-17, and around 20 s, significantly larger than that at SKR with the energy primarily concentrated around 10 s. Therefore, wave motion recorded at YPT will have larger influence than that at SKR on structures with period longer than 2.2 s (inverse of 0.45 Hz), i.e., flexible structures such as high-rise buildings and long-span bridges. This is consistent with the curves in Fig. 9. Similarly, since the seismic energy at YPT with frequency in 0.55-0.9 Hz (primarily concentrated in 5-13 s) is much larger than that at SKR in the same frequency range, the motion at YPT will also have larger influence on structures with period between 1.1 and 1.8 s (reciprocal of 0.9 and 0.55 Hz), i.e., most intermediate-high buildings and standard bridges. In short, the temporal-frequency seismic energy of the EMD-low measurements in other frequency range in Fig. 10a,b is consistent with the spectral responses in Fig. 9.
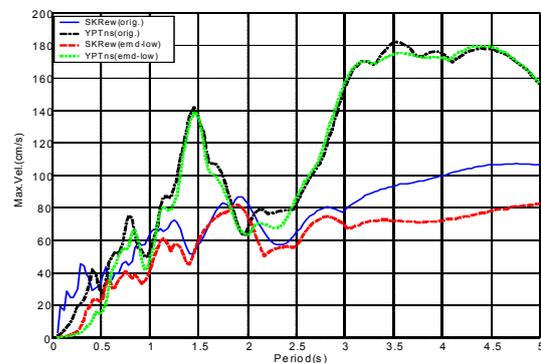
Fig. 9   Comparison of velocity response spectra with 5% damping using the original and EMD-based low-frequency accelerations at SKR and YPT.
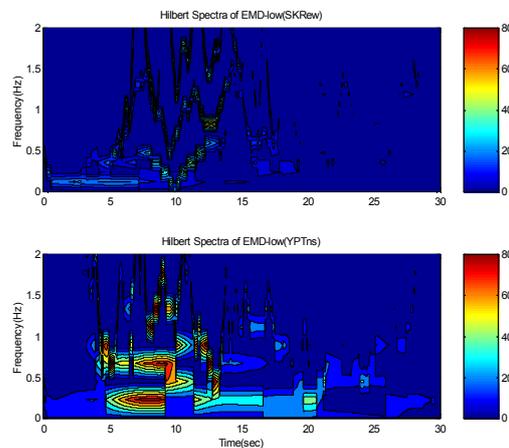
Fig. 10a,b (a, top) Hilbert spectrum of EMD-based low-frequency acceleration in the east-west component at SKR, (b, bottom) Hilbert spectrum of EMD-based low-frequency acceleration in the north-south component at YPT.

Following this approach, we analyze three other pairs of the earthquake recordings, each of which is comparably distant from the fault. The results show that the EMD-low measurements and their peaks are particularly consistent with

the responses of structures with period ranging from 0.5 to 2 s. This suggests that the peak of EMD-low measurement is likely a more appropriate index than is the PGA of original recording in estimating a motion's potential to cause damage to most civil structures with intermediate-to-long period.

4.2 Representation of Low-frequency Pulse-like Waves

The high-energy single or multiple pulses observed near the beginning of velocity time histories have recently been found to be important features of near-source motion in seismological and engineering studies [1,2,4,7,8,14,15]. The 1999 Kocaeli Turkey earthquake recordings show such near-source velocity-pulse waves, representative of low-frequency pulse-like (LFPL) wave features of ground motion.

Depicted in Fig. 7b is the velocity recording at SKR, obtained by integrating the acceleration recording. The velocity-based LFPL wave signals can be well approximated by the currently-used triangle-type single-pulse [3]. Similarly, the LFPL waves in the velocity recording at YPT in Fig. 8b can also be well described by multiple pulses. These velocity-based LFPL waves or their approximation integrate important information contained in the ground motion such as the dominant low-frequency content comparable to the fundamental natural frequencies of most civil structures, the peak amplitudes, and non-stationarity of the motion. In addition, the area of LFPL waves over time in the velocity time history is a cumulative measure of seismic energy to which the velocity squared is proportional. Likely because of the above features, the velocity-based LFPL waves are regarded as one of the major contributors to the destruction of structural and geotechnical engineering systems in earthquakes [16]. They are also typically regarded as a better measure of a motion's potential to cause damage to civil structures than are others such as PGA.

While the above observation is generally true, in the following two sub-sections we illustrate that LFPL waves extracted from velocity recordings are not as direct a measure of motion's potential for causing structural damage as is the motion represented in EMD-low measurement extracted directly from acceleration recordings.

4.2.1 Velocity-based versus acceleration-based pulses

Since velocity time histories are obtained from acceleration recordings, the estimate waveforms might be distorted by data processing, such as baseline correction, bandpass filtering, and instrument correction. More important, with few exceptions, the input forces to a structural system in structural dynamic analysis are proportional to acceleration, not velocity. This can be seen from the governing equation of a SDOF structure,

$$m\ddot{x} + f_d(\dot{x}) + f_r(\dot{x}, x) = -m\ddot{y} \qquad (1)$$

where m is the mass of the structure, x and y are respectively the structural displacement relative to the ground and ground displacement, f_d and f_r are respectively the damping and restoring forces of the structure, and dot stands for the derivative with respect to time.

Since the EMD-low measurements are extracted directly from acceleration recordings and contain the information most directly related to the motion and dynamic characteristics of structures (e.g., comparable frequency content, motion's non-stationarity, a good representative of LFPL waves for the acceleration recording), they might be more appropriate than measurements obtained from velocity recordings.

Figures 7c and 8c show the EMD-low accelerations, while Figs. 7d and 8d show the accelerations obtained by differentiating the triangle-type velocity pulses in Figs. 7b and 8b. Comparing these two sets of accelerations with the pertinent original acceleration recordings in Figs. 7a and 8a indicates that the EMD-low measurements can capture the essence of LFPL waves in acceleration recordings better than do the velocity-pulse-based accelerations.

It is of interest to note that the velocity-based LFPL waves have their seismological value as well. For example, the peak and period of the triangle-type LFPL waves or their approximation in velocity are directly related to the earthquake magnitude, the rise-time, and the shortest distance from the site to the fault [17]. Nevertheless, we focus on implications of the LFPL wave representation on structural damage, not on its relationship to the seismic source. Accordingly, quantities seen in the EMD-low measurements (e.g., the peak) are likely more appropriate indices for predicting a motion's potential for causing structural damage than are others such as PGV obtained in velocity recordings.

4.2.2 Seismic energy at site versus input to structures

Since velocity squared is proportional to energy, the larger the area beneath the velocity-based LFPL measurements or their approximation over time, the larger the cumulative seismic energy. However, this energy is an intensity measure of the ground motion at one site, not the measure of the motion's input to a structural system. Following [21], we explain it as follows. Multiplying Eq. (1) by dx and integrating from 0 to x, we obtain

$$\int_0^x m\ddot{x}\,dx + \int_0^x f_d(\dot{x})dx + \int_0^x f_r(\dot{x}, x)dx = -\int_0^x m\ddot{y}\,dx \qquad (2a)$$

or equivalently

$$E_k(\dot{x}) + E_d(\dot{x}) + E_p(\dot{x}, x) = E_i(x) \quad , \qquad (2b)$$

where E, with subscripts k, d, p and i, denote respectively the kinetic, damping, potential and input energy. Equation (2a) or (2b) indicates that the seismic energy input to a structural system is not simply proportional to velocity or its square. Therefore, the area of LFPL wave measurement or their approximation in velocity is not the proper measure of seismic energy input to a structural system (although it is a proper measure of motion at certain location related to the energy released by a seismic source and site amplification).

To demonstrate the above point, the area beneath the velocity pulses at SKR and YPT in Figs. 7b and 8b are calculated as 212.8 cm^2 (272.5 cm^2 for triangle pulses), which is larger than 176.8 cm^2 (223.1 cm^2 for triangle pulses) at YPT. This likely suggests, among others, that the seismic energy at SKR is larger than that at YPT, which is of importance in addressing such seismological issues as seismic energy attenuation in the earth or local site amplification. The motion

with a larger area, however, does not necessarily mean that its potential to cause damage to a structural system is also greater. In fact, the response spectra to these two recordings in Fig. 9 show opposite results.
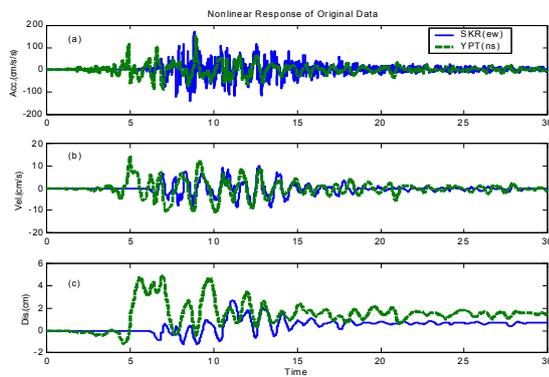
Fig. 11a-c   Non-linear response time histories of (a, top) acceleration, (b, middle) velocity, and (c, bottom) displacement to the recordings at YPT and SKR.
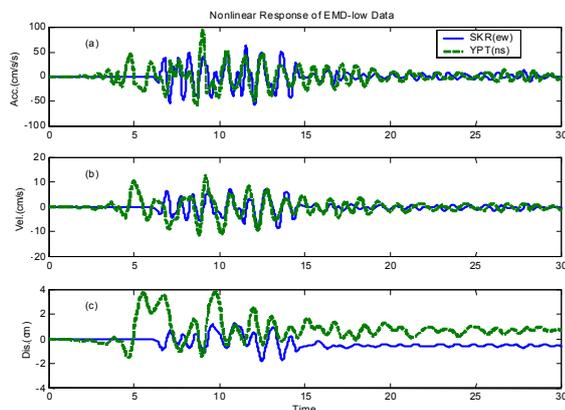
Fig. 12a-c   Non-linear response time histories of (a, top) acceleration, (b, middle) velocity, and (c, bottom) displacement to the EMD-based low-frequency components of recordings at YPT and SKR.
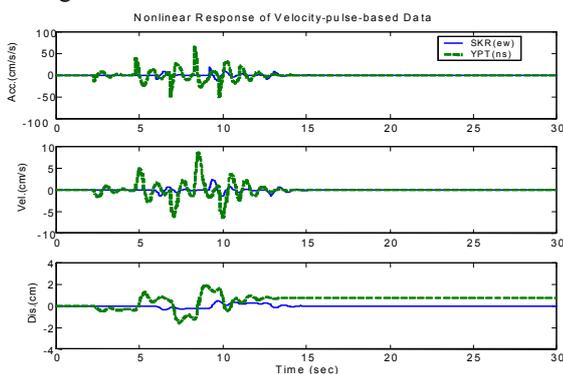
Fig. 13a-c   Non-linear response time histories of (a, top) acceleration, (b, middle) velocity, and (c, bottom) displacement to the velocity-pulse-based acceleration of recordings at YPT and SKR.
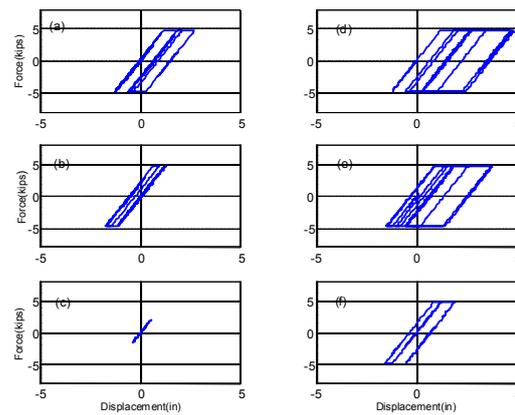
Fig. 14a-f Time histories of elasto-plastic stiffness due to (a) recording at SKR (shown in Fig. 7a), (b) EMD-based low-frequency component of recording at SKR (shown in Fig. 7c), (c) velocity-pulse-based acceleration at SKR (shown in Fig. 7d), (d) recording at YPT (shown in Fig. 8a), (e) EMD-based low-frequency component of recording at YPT(shown in Fig. 8c), and (f) velocity-pulse-based acceleration at YPT(shown in Fig. 8d).

To further clarify this point, we have calculated the nonlinear structural responses of a SDOF system to the two recordings. In particular, a nonlinear SDOF [19] is selected with the structural parameters: m=0.1 $kips \cdot s^2/in$, c=0.2 $kips \cdot s/in$, k_e=5 $kips/in$, k_p=0 at $|f_r| \geq 6$ $kips$, where k_e and k_p are respectively the elastic and plastic stiffness. The time histories of acceleration, velocity and displacement responses, shown in Figs. 11a,b,c, indicate that the recording at YPT will cause larger structural responses in the intermediate- to low-frequency range (velocity and displacement) than those that at SKR. This supports our previous response spectral analysis. Comparison of the time histories of responses to EMD-based and velocity-pulse-based accelerations in Figs. 12a,b,c and 13a,b,c with those in Figs. 11a,b,c show that the EMD-based measurement much better characterizes a motion's action on structures than does velocity-pulse-based acceleration. This is also illustrated in Fig. 14, which shows the force-displacement relationships among the recording, EMD-based and velocity-pulse-based accelerations.

4.3 Attenuation Formulae for HHT-based Motion Features

The above observations suggest that the peak of EMD-low measurement is likely more closely correlated with structural damage than are other characteristic measures of ground motion such as PGA, PGV, velocity-based LFPL waves, although this statement needs further validation by examining other ground motion data sets. Accordingly, alternative to or complementary to the existing measure of ground motion such as the equation for estimating horizontal PGA [18] and its use in Kocaeli earthquake [16], the peak of the EMD-low acceleration can be regarded as a new measure for a motion's potential for destruction of certain type of structural and geotechnical engineering systems in the 1999 Kocaeli Turkey Earthquake and the others. Figure 15 shows the attenuation relationship between the peak of original or EMD-low

accelerations and the distance to the fault trace. The data are fit by an exponential function instead of an empirical function form of PGA attenuation relationships [16]. The exponential attenuation formula for the peak of EMD-low accelerations has smaller scatter than does that for the peak of the original data. This supports the above-mentioned merits that the peak of EMD-based recording is likely more consistent with structural responses and damage potential to structures than is the PGA of the original data.
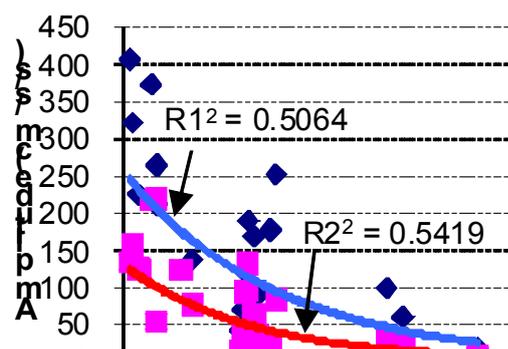
Fig. 15   Attenuation curve for peak of EMD-based acceleration as a function distance from the fault. $R1^2$ and $R2^2$ are measures of scatter of the discrete data for peaks of original and EMD-based accelerations from the pertinent fitting curves, e.g., the larger the R^2, the smaller scatter.

V.   Summary

This study investigates the rationale of the method of HHT for earthquake data analysis and its subsequent application to studies of earthquake engineering and seismology. It reveals the following:

(1)   Conventional data processing techniques are found to be less suited for analyzing nonlinear, non-stationary earthquake recordings than is the HHT method.

(2)   The decomposed components in HHT, namely the Intrinsic Mode Functions (IMF), likely extract more pertinent information from the original data than do Fourier-based and wavelet components.   Based on analysis of the 1994 Northridge earthquake [20] as an example, the dominant IMF components of the earthquake recordings are found well correlated to its source heterogeneity and rupture process.

(3)   The motion of grouped low-frequency IMF components, i.e., EMD-based low-frequency recording, is more suitable for characterizing the influences of LFPL waves in structural dynamic responses than is the conventional velocity-based pulse-wave motion. From the perspective of seismic-induced structural damage, its peak is a more appropriate individual measure of ground motion features than are the traditional measures such as PGA or PGV.

Acknowledgment

References

[1]   J.F. Hall, Heaton, T.H., Halling, M.W. and Wald, D.J. "Near-source ground motion and its effects on flexible buildings," *Earthquake Spectra*, 11(4), 1995, 569-605.

[2]   T.H. Heaton, Hall, J.F., Wald, D.J. and Halling, M.W. "Response of high-rise and base-isolated buildings to a hypothetical Mw 7.0 blind thrust earthquake," *Science*, 267, 1995, 206-211.

[3]   P.G. Somerville and Graves, R.W. "Ground motions: site response and near-fault effects," *Tall Building Structures-A World View*, 1996, 169-185.

[4]   P. Somerville "Engineering characteristics of near fault ground motion," *SMIP97 Seminar on Utilization of Strong-Motion Data,* Los Angeles, CA, 1997.

[5]   S. Hartzell "Variability in nonlinear sediment response during the 1994 Northridge, California, earthquake," *Bull. Seism. Soc. Am.* 88, 1998, 1426-1437.

[6]   S. Hartzell, S. Harmsen, A. Frankel, and S Larsen "Calculation of broadband time histories of ground motion: Comparison of methods and validation using strong-ground motion from the 1994 Northridge earthquake," *Bull. Seism. Soc. Am.* 89, 1999, 1484-1504.

[7]   M. Shinozuka, Deodatis, G., Zhang, R. and Papageorgiou, A.S. "Modeling, synthetics and engineering applications of strong earthquake wave motion," *Journal of Soil Dynamics and Earthquake Engineering*, 18(3), 1999, 209-228.

[8]   B. Alavi and Krawinkler, H. "Consideration of near-fault ground motion effects in seismic design," in CD-ROM, *Proceedings of 12 WCEE*, 2000.

[9]   N.E. Huang, S. Zheng, S.R. Long, M.C. Wu, H,H. Shih, Q. Zheng, N-C. Yen, C.C. Tung, and M.H. Liu. "The empirical mode decomposition and Hilbert spectrum for nonlinear and nonstationary time series analysis." *Proceedings of Royal Society of London, A* 454, 1998, 903-995.

[10]   N.E. Huang, Z. Shen, and R.S. Long, "A new view of nonlinear water waves--Hilbert Spectrum". *Ann. Rev. Fluid Mech*. 31, 1999, 417-457.

[11]   R. Zhang, S. Ma, E. Safak, and S. Hartzell, "Hilbert-Huang transform analysis of dynamic and earthquake motion recordings," *ASCE Journal of Engineering Mechanics,* 129, 8, 2003, pp 861-875.

[12]   S. Hartzell, Liu, P., and Mendoza, C. (1996) "The 1994 Northridge, California, earthquake: Investigation of rupture velocity, risetime, and high-frequency radiation," *J. of Geophys. Res*., 101, 1996, 20091-20108.

[13]   A.H. Olson, J.A. Orcutt and G.A. Frazier "The discrete wavenumber/finite element method for synthetic seismograms," *Geophys. J. R. Astron. Soc.*, 77, 1984, 421-260.

[14]   W. Iwan "Drift spectrum: Measure of demand for earthquake ground motions," *ASCE Journal of Engineering Mechanics*, 123(4), 1997, 397-406.

[15]   M. Sasani and Bertero, V.V. "Importance of severe pulse-type ground motions in performance-based engineering: historical and critical review," in CD-ROM, *Proceedings of 12 WCEE*, 2000.

[16]   USGS (2000). "Implications for Earthquake Risk Reduction in the United States from the Kocaeli, Turkey, Earthquake of August 19, 1999," *USGS Circular 1193*, 2000.

[17]   P. Somerville (1998). "Development of an improved representation of near-fault ground motions," *SMIP98 Seminar on Utilization of Strong-Motion Data,* Oakland, CA, 1998.

[18]   D.M. Boore, Joyner, B.J., and Fumal, T.E. (1997) "Equation for estimating horizontal response spectra and peak acceleration from western north American earthquakes: a summary of recent work," *Seismological Research Letters*, 68(1), 1997, 128-151.

[19]   R.W. Clough and J. Penzien (1993). *Dynamics of Structures*, Second Edition, McGraw-Hill, Inc., New York, 1993.

[20]   R. Zhang, S. Ma, and S. Hartzell, "Signatures of the seismic source in EMD-based characterization of the 1994 Northridge, California,

earthquake recordings," *Bulletin of the Seismological Society of America*, 93(1), 2003, 501-518.

[21] A.K. Chopra *Dynamics of Structures: Theory and Applications to Earthquake Engineering*, Prentice Hall, Upper Saddle River, New Jersey, 1995.

[22] A. Toma, "The Fourier Transform of some distributions from D0(R) and D0(R2) with applications in mechanics" *Recent Advances in Acoustics & Music,* Proceedings of the 11th WSEAS International Conference on Acoustics & Music: Theory & Applications (AMTA '10), "G. Enescu" University, Iasi, Romania, June 13-15, 2010. ISBN: 978-960-474-192-2 / ISSN: 1790-5095, pp 51-54.

[23] C. Guarnaccia, "Acoustical Noise Analysis in Road Intersections: a Case Study" *Advances in Acoustics $ Music,* Proceedings of the 11th WSEAS International Conference on Acoustics & Music: Theory & Applications (AMTA '10), "G. Enescu" University, Iasi, Romania, June 13-15, 2010. ISBN: 978-960-474-192-2 / ISSN: 1790-5095, pp 208-215.

[24] V.N. Ivanovic and S. Jovanovski, "Signal Adaptive Method for Improved Space/Spatial-Frequency Representation of Nonstationary Two-Dimensional Signals" *New Aspects of Signal Processing,* Proceedings of the 9th WSEAS International Conference on Signal Processing (SIP '10), Catania, Italy, May 29-31, 2010. ISBN: 978-954-92600-4-5 / ISSN: 1790-5117, pp 72-76.

[25] S. Abdullahi, T.E. Putra, M.Z. Nuawi, Z.M. Nopiah, A. Arifin and L. Abdullah, "Time-Frequency Localisation Analysis for Extracting Fatigue Damaging Events," *Recent Advances in Signal Proccessing, Robotics and Automation*, Proceedings of the 9th WSEAS International Conference on Signal Processing, Robotics and Automation (ISPRA '10), University of Cambridge, UK, February 20-22, 2010. ISBN: 978-960-474-157-1 / ISSN: 1790-5117, pp 31-35.

Ray Ruichong Zhang received his B.S degree in engineering mechanics in 1984, M.S degree in structural engineering in 1987, both from Tongji University, Shanghai, China, and Ph.D. degree in mechanical engineering from Florida Atlantic University, Florida, USA in 1992. He is registered Professional Engineer in California, USA.

He holds Associate Professorship in Division of Engineering at Colorado School of Mines, Golden, Colorado, USA. Before joining Colorado School of Mines, Dr. Zhang had worked in Princeton University for three and a half years as Post-Doctoral Research Associate, and in University of Southern California for two years as Research Assistant Professor. He also took sabbatical leave from Colorado School of Mines and worked as Visiting Associate Professor in Department of Mechanical Engineering at Petroleum Institute, Abu Dhabi, United Arab Emirates in 2009-2010, in addition to his working as visiting scholar in Tongji University, Hong Kong Polytechnic University and Tianjing University in China in the summer of 2000, 2001 and 2003 respectively.

Dr. Zhang's research interest resides in continuum mechanics, vibration theory, wave propagation, stochastic processes and fields, and advanced data processing and analysis for sensory systems, disaster assessment and mitigation, and structural/geotechnical nondestructive evaluation and health monitoring. He is author of one edited book, one book chapter, one edited journal, thirty nine journal papers and numerous papers in conference proceedings and edited books. Dr. Zhang is the recipient of 1997 IASSAR Junior Research Prize in Stochastic Dynamics for his contribution to the solutions of seismic wave propagation through stochastic media, bestowed by International Association for Structural Safety and Reliability (IASSAR).

Ray Ruichong Zhang: rzhang@mines.edu